ACS APPLIED MATERIALS & INTERFACES

Research Article

www.acsami.org

Facile Fabrication of Highly Efficient g-C_3N_4/Ag_2O Heterostructured Photocatalysts with Enhanced Visible-Light Photocatalytic Activity

Miao Xu,[†,‡] Lei Han,[†,‡] and Shaojun Dong*[,†,‡]

[†]State Key Laboratory of Electroanalytical Chemistry, Changchun Institute of Applied Chemistry, Chinese Academy of Science, Changchun, Jilin 130022, P. R. China

[‡]University of Chinese Academy of Sciences, Beijing 100049, P. R. China

Supporting Information

ABSTRACT: Highly efficient visible-light-driven g-C_3N_4/Ag_2O heterostructured photocatalysts were prepared by a simple liquid phase synthesis method at room temperature. The composition, structure, morphology, and optical absorption properties of the as-prepared g-C_3N_4/Ag_2O composites were characterized by XRD, FTIR, XPS, TEM, and UV−vis DRS, respectively. We found interestingly that the photogenerated charge carriers separations of the as-prepared g-C_3N_4/Ag_2O composites were closely related to the mass ratio of g-C_3N_4 and Ag_2O. When the mass ratio of g-C_3N_4 and Ag_2O reached 1:4, the as-prepared composite exhibited the highest photocatalytic activity, which was almost 11 and 1.2 times as high as that of individual g-C_3N_4 and Ag_2O, respectively. The enhancement of photocatalytic activity could be attributed to the synergetic effects between g-C_3N_4 and Ag_2O as well as the improved dispersibility and the decreased particle size of Ag_2O. Moreover, the as-prepared composites showed excellent stability toward the photodegradation of methyl orange (MO). Finally, a possible photocatalytic and charge separation mechanism was proposed.

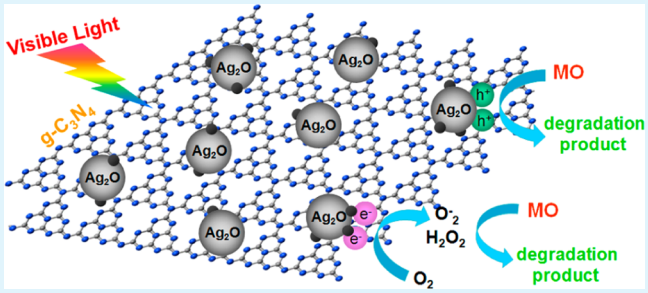

KEYWORDS: *heterostructure, g-C_3N_4, Ag_2O, visible-light photocatalysis*

1. INTRODUCTION

Heterogeneous photocatalysis has been recognized as a potential strategy for solar energy conversion and environmental remediation. Of the well-known semiconductor photocatalysts, TiO_2 has been proved to be the most representative and extensively used material owing to its chemical and physical inertness, nontoxicity, and low-cost.[1] However, the low solar energy conversion efficiency greatly restricts its practical application because of its wide band gap. Although there are many strategies to extend the optical absorption of TiO_2,[2−8] the enhancement of the visible-light photocatalytic activity is still very limited. Therefore, it is still a great challenge and highly crucial to explore novel photocatalytic materials with visible-light response, such as Ag-based photocatalysts.[9,10]

Graphitic carbon nitride (g-C_3N_4), a polymeric metal-free semiconductor with a band gap of about 2.70 eV, has been recently focused on the photocatalytic field, which fulfills the basic requirements as a photocatalyst for water splitting and/or organic pollutant decomposition,[11−14] including being abundant, stable, and responsive to visible-light. Nevertheless, the lack of absorption above 460 nm, the low quantum efficiency, and the fast recombination of photogenerated electeon-hole pairs may still limit the enhancement of its photocatalytic activity. Therefore, some strategies have been devoted to improving the photocatalytic activity of g-C_3N_4, such as nano/mesoporous structures fabrication,[15−17] transition metal modification,[18] heterostructured composite fabrication,[19−23] and so forth. In particular, the fabrication of heterostructured composites by combining g-C_3N_4 with other semiconductors can not only restrict efficiently the recombination of photogenerated charge carriers, but also endow the composites novel characteristics or some enhanced properties by the synergistic effects or antagonistic effects.

On the other hand, Ag_2O as a *p*-type semiconductor has been found to be a self-stable and highly efficient visible-light photocatalyst with a narrow energy bandgap of ∼1.3 eV.[24] And it has been widely used as sensitizer to tune the light response of some wide bandgap semiconductors into the visible region and enhance their photocatalytic activity, such as Ag_2O/TiO_2 nanobelts,[25] Ag_2O/ZnO,[26] Ag_2O/Bi_2WO_6,[27] and so forth. The combination of g-C_3N_4 and Ag_2O that possesses well matched overlapping band structure can easily fabricate a *p*−*n* heterojunction, which will bring more effective interface transfer of photogenerated electrons and holes in comparison with the traditional composites. Furthermore, Ag_2O nanoparticles are dispersed on the surface of g-C_3N_4, which can greatly reduce the usage of Ag for enhanced photocatalytic activity.

Received: September 5, 2013
Accepted: November 8, 2013
Published: November 8, 2013

   dx.doi.org/10.1021/am4038307 | ACS Appl. Mater. Interfaces 2013, 5, 12533−12540

Herein, highly efficient visible-light-driven heterostructured photocatalysts, g-C_3N_4/Ag_2O, were prepared by a simple liquid phase reaction at room temperature. The novel heterostructured photocatalysts possessed better photocatalytic activity and stability toward the photodegradation of methyl orange (MO) under visible light irradiation compared with the pure g-C_3N_4 and Ag_2O. Meanwhile, we also proposed a possible mechanism for the enhanced activity of g-C_3N_4/Ag_2O composites on account of the experimental results.

2. EXPERIMENTAL SECTION

2.1. Materials. Melamine ($C_3H_6N_6$) was obtained from Sinopharm Chemical Reagent Corp, P. R. China. Silver nitrate ($AgNO_3$) and sodium hydroxide (NaOH) were purchased from Beijing Chemical Works, P. R. China. All chemicals were used as received without further purification, and all aqueous solutions were prepared with ultrapure water (>18.25 MΩ cm) obtained from Millipore system.

2.2. Synthesis of g-C_3N_4. The g-C_3N_4 power was synthesized according to the literature.[28] Typically, 10 g of melamine was put into an alumina crucible with a cover and heated at a rate of 2 °C min^{-1} to 550 °C in a muffle furnace and then kept at this temperature for 4 h. All the experiments were performed under air conditions. The resulting yellow product was collected and ground into powder for further use.

2.3. Fabrication of g-C_3N_4/Ag_2O Composite Photocatalysts. The typical preparation procedure of the g-C_3N_4/Ag_2O composite photocatalysts was as follows: 0.15 g of g-C_3N_4 was added into 30 mL of distilled water and sonicated for 30 min. Then, 0.6 g to NaOH was added into the suspension and stirred for 30 min. Further, 13 mL of 0.1 M $AgNO_3$ was added drop by drop under stirring, and the mixture was held in the dark for 30 min with continuous stirring. All the experiments were carried out at room temperature. The obtained precipitate was collected by centrifugation and washed with distilled water for three times. Finally, the solid product was dried at 60 °C overnight. A series of g-C_3N_4/Ag_2O composites with different mass ratios of g-C_3N_4 and Ag_2O were prepared by changing the amounts of g-C_3N_4 and marked as 4:1, 1:1, 1:4, and 1:16. As a reference, the pure Ag_2O was prepared without adding g-C_3N_4 under the same conditions. Moreover, a mechanically mixed sample (the mass ratio of g-C_3N_4 and Ag_2O was 1:4) was obtained by grinding 0.2 g of g-C_3N_4 with 0.8 g of Ag_2O.

2.4. Characterization. The X-ray diffraction (XRD) measurements were performed on a D8 Focus diffractometer (Bruker) with Cu Kα radiation (λ = 0.15405 nm) in the range of 10−80° (2θ). Infrared spectra were collected on a VERTEX 70 Fourier transform infrared (FTIR) spectrometer (Bruker). X-ray photoelectron spectroscopy (XPS) analysis was carried on an ESCALAB MK II X-ray photoelectron spectrometer. UV−vis diffuse-reflectance spectra (UV−vis DRS) were obtained on an UV−vis spectrophotometer (UV-2550, Shimadzu, Japan). $BaSO_4$ was used as a reflectance standard in the UV−vis diffuse-reflectance experiments. Transmission electron microscopy (TEM) and high-resolution transmission electron microscopy (HRTEM) images were obtained with a TECNAI G2 high-resolution transmission electron microscope operating at 200 kV. Scanning electron microscope (SEM) images were taken with a XL30 field-emission scanning electron microscope at an accelerating voltage of 15 kV. Photoluminescence (PL) spectra were measured at room temperature on an F-7000 fluorescence spectrophotometer (Hitachi, Japan) with an excitation wavelength of 325 nm. The scanning speed was 1200 nm min^{-1}, and the photomultipliers voltage was 700 V. The widths of the excitation and emission slits were both 5.0 nm. UV−vis absorbance measurements were performed on a Cary 500 Scan UV/vis/NIR spectrophotometer (Varian).

2.5. Evaluation of Photocatalytic Activity. The photocatalytic activities of the as-prepared photocatalysts were evaluated by the degradation of the methyl orange (MO) aqueous solution under visible light irradiation. In order to exclude the effect of photosensitivity, phenol as a typical colorless pollutant was also degraded by the as-prepared composites for evaluating the photocatalytic activity. The light source was a 300 W xenon lamp (PLS-SXE300, Beijing Trusttech Co. Ltd., China) with a UV-cut filter ($\lambda \geq$ 400 nm). In a typical experiment, 20 mg of the powdered photocatalyst was suspended in 50 mL of 20 mg L^{-1} MO (or phenol) aqueous solution. Prior to light irradiation, the dispersion was first sonicated for 10 min and then stirred magnetically in the dark for 30 min to reach the adsorption−desorption equilibrium of dye molecules on the catalyst. The specified dispersions were pipetted at the given time intervals and centrifuged at 10 000 rpm for 5 min. The concentration of the MO (or phenol) aqueous solution was monitored using a UV−vis spectroscopy. The absorbance of MO and phenol were determined by the peak at 463 and 270 nm respectively, while the change in concentration was recorded as C/C_0 (C_0 was the initial concentration of MO (or phenol) aqueous solution, and C was the concentration at time t). The direct photolysis experiment of MO (or phenol) was carried out without the addition of the catalyst under the same conditions.

3. RESULTS AND DISCUSSION

3.1. Structure and Composition of g-C_3N_4/Ag_2O Photocatalysts. The structure and composition of the as-prepared samples were characterized by XRD, FTIR and XPS, respectively. XRD patterns of the as-prepared g-C_3N_4/Ag_2O composites with different mass ratios are shown in Figure 1,

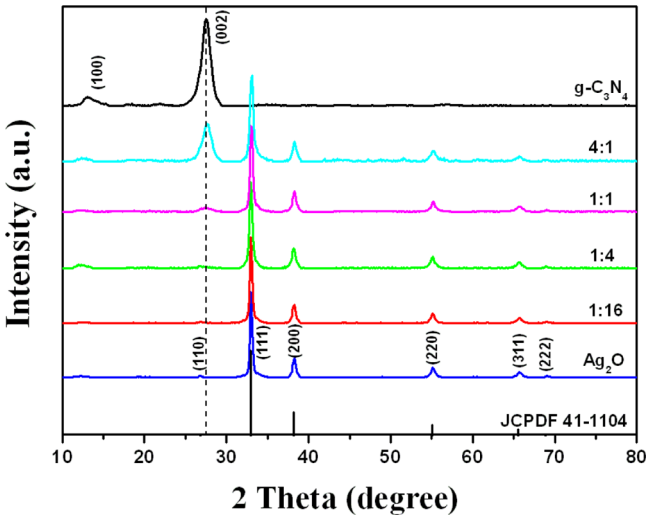

Figure 1. XRD patterns of the as-prepared g-C_3N_4, Ag_2O, and g-C_3N_4/Ag_2O composites.

together with the patterns of pure g-C_3N_4 and Ag_2O. For the pure g-C_3N_4 sample, the characteristic peak at 27.5° corresponds to the (002) plane arising from the stacking of the conjugated aromatic system.[11] The diffraction peaks of pure Ag_2O are indexed to the (110), (111), (200), (220), (311), and (222) planes of the cubic crystal phase (JCPDS 41-1104).[24] In the g-C_3N_4/Ag_2O composite with the mass ratio of 1:16, no diffraction peaks of g-C_3N_4 can be found owing to the relatively low percentage of g-C_3N_4. With increasing the mass ratio of g-C_3N_4 and Ag_2O from 1:4 to 4:1, the typical diffraction peak of g-C_3N_4 gradually appears and no other diffraction peaks are detected except the peaks of g-C_3N_4 and Ag_2O. The results indicate that a coexistence of Ag_2O and g-C_3N_4, and no impurities are formed during the fabrication of the composites. Moreover, when the g-C_3N_4 content is high (>50%), the weak peak of Ag_2O at 26.7° may be covered by the strong peak of g-C_3N_4 at 27.5° and cannot be observed in the XRD patterns.

The existence of g-C_3N_4 and Ag_2O in the as-prepared samples was further confirmed by FTIR analysis. Figure 2

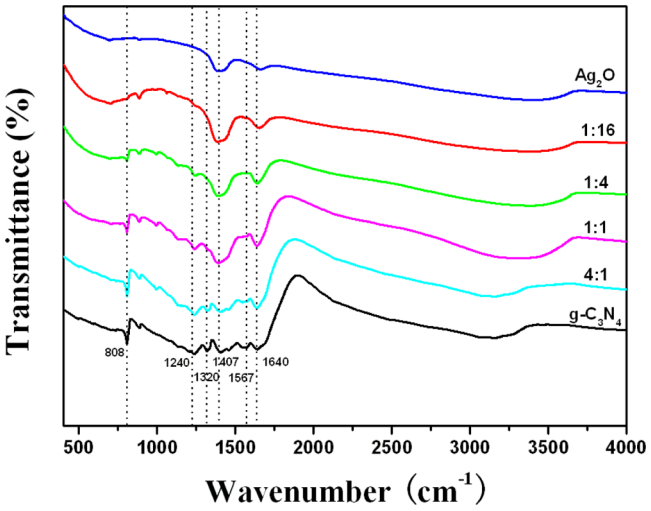

Figure 2. FTIR spectra of the as-prepared g-C_3N_4, Ag_2O, and g-C_3N_4/Ag_2O composites.

shows the FTIR spectra of the pure Ag_2O, pure g-C_3N_4, and a series of g-C_3N_4/Ag_2O composite photocatalysts, respectively. For the pure g-C_3N_4, three main absorption regions can be observed clearly. The broad peak at 3000−3500 cm^{-1} is ascribed to the stretching vibration of N−H and the stretching vibration of O−H of the physically adsorbed water.[28−30] The strong band of 1200−1700 cm^{-1}, with the characteristic peaks at 1240, 1320, 1407, 1567, and 1640 cm^{-1}, is attributed to the typcial stretching vibration of CN heterocycles.[28] In addition, the peak at 808 cm^{-1} can correspond to the breathing mode of triazine units.[28,30] For the pure Ag_2O, the observed broad peak around 3500 cm^{-1} and the peak at 1661 cm^{-1} belong to the O−H stretching vibration, while the peak at 1386 cm^{-1} belongs to the H−O−H bending vibration of the adsorbed water molecules on the surface.[31] Furthermore, the broad absorption peak around 600 cm^{-1} is related to Ag−O bond vibration.[32,33] The FTIR spectra of the g-C_3N_4/Ag_2O composites represent the overlap of the spectra of both g-C_3N_4 and Ag_2O. It should be noted that the intensity of the peak at 808 cm^{-1} decreases with the decrease of the g-C_3N_4 content.

The composition and chemical status of the as-prepared samples were also confirmed by XPS technique. Figure 3 displays the XPS survey spectra of the pure Ag_2O, g-C_3N_4, and the prepared g-C_3N_4/Ag_2O (1:4) composite photocatalyst. Compared with bare Ag_2O and g-C_3N_4, the composite is composed of Ag, O, N, and C elements. The typical high resolution XPS spectra of Ag 3d, O 1s, C 1s, and N 1s in the g-C_3N_4/Ag_2O (1:4) composite are also shown in Figure 4. The doublet peaks of Ag $3d_{5/2}$ and Ag $3d_{3/2}$ are, respectively, located at about 368.4 and 374.4 eV, which are very close to the binding energy values of Ag^+ in Ag_2O (Figure 4A).[27] The asymmetric O 1s peak shown in Figure 4B can be split by using the XPS peak-fitting program. The peak at 532.6 eV is assigned to the external −OH group or the water molecule adsorbed on the surface, and the other O 1s peak appearing at 531.0 eV corresponds to lattice oxygen atoms in the Ag_2O.[34] The results further indicate the existence of Ag_2O phase in the composite, which is in good agreement with the XRD and FTIR results. Figure 4C shows the high resolution C1s spectrum of the

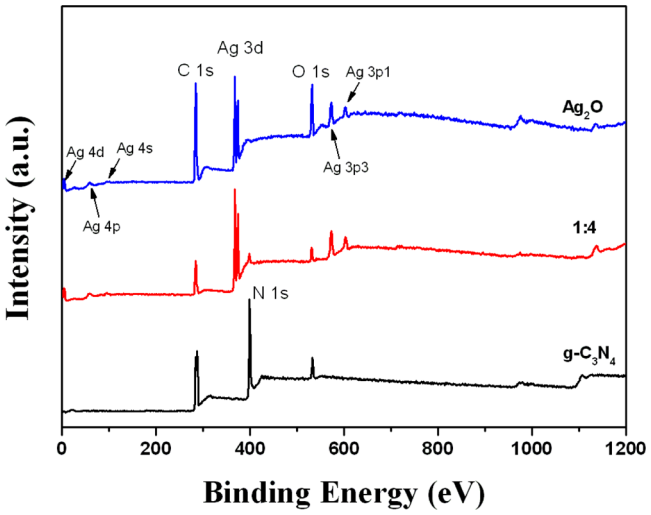

Figure 3. XPS survey spectra of the as-prepared g-C_3N_4, Ag_2O, and g-C_3N_4/Ag_2O (1:4) composites.

composite. The peak centered at 284.6 eV can be ascribed to the C−C coordination of the surface adventitious carbon, whereas the peak at 288.1 eV corresponds to sp^3-bonded C in C−N of g-C_3N_4.[23,35,36] The N 1s peak XPS spectrum is deconvoluted into three Gaussian−Lorenzian peaks centered at 398.9, 400.2, and 404.5 eV (Figure 4D), which can be attributed to the pyridinic-like nitrogen (N−sp^2C), graphitic nitrogen (N−$(C)_3$), as well as the charging effects, respectively, in accordance with the reported results.[23,36] Furthermore, the binding energy values of Ag 3d and N 1s in the composite are slightly higher than those of pure Ag_2O and pure g-C_3N_4 (Figure S1, Supporting Information). The shift can be ascribed to the strong interaction between Ag_2O and g-C_3N_4. The above investigations strongly confirm that the as-prepared composite including both g-C_3N_4 and Ag_2O forms the heterostructure rather than the physical mixture.

3.2. Morphology of g-C_3N_4/Ag_2O Photocatalysts.

Figure 5 shows the TEM images of the pure g-C_3N_4 and the g-C_3N_4/Ag_2O composite photocatalyst with the mass ratio of 1:4. For comparison, the composites with different ratios of g-C_3N_4 and Ag_2O and pure Ag_2O were also characterized by TEM and SEM shown in Figures S2 and S3, respectively. From Figure 5A, the as-prepared g-C_3N_4 sample reveals a clearly flat layer structure, which is in agreement with the previous report.[37] After the introduction of Ag_2O, numerous dark Ag_2O particles appear on the lamellar g-C_3N_4 (Figure 5B) and the size of Ag_2O particles is about 5−30 nm. All the Ag_2O particles are attached to the surface of g-C_3N_4 strongly. The HRTEM image of the as-prepared g-C_3N_4/Ag_2O photocatalysts was displayed (Figure 5B, inset). By measuring the lattice fringes, the interplanar spacing is about 0.27 nm, corresponding to the (111) plane of Ag_2O (JCPDS 41-1104). The result of the HRTEM image also clearly reveals a close interface between the Ag_2O and g-C_3N_4 in the as-prepared composite and indicates the formation of heterojunction,[34] which is significant for separating the photogenerated electron−hole pairs and thus improving the quantum efficiency. As shown in Figure S3, for pure Ag_2O, the Ag_2O nanoparticles agglomerate and the size of Ag_2O nanoparticles is about 100−200 nm. The addition of g-C_3N_4 can greatly improve the dispersibility of Ag_2O particles and efficiently decrease the particle size of Ag_2O (Figure S2). Both of them should be significant for increasing the charge

dx.doi.org/10.1021/am4038307 | ACS Appl. Mater. Interfaces 2013, 5, 12533−12540

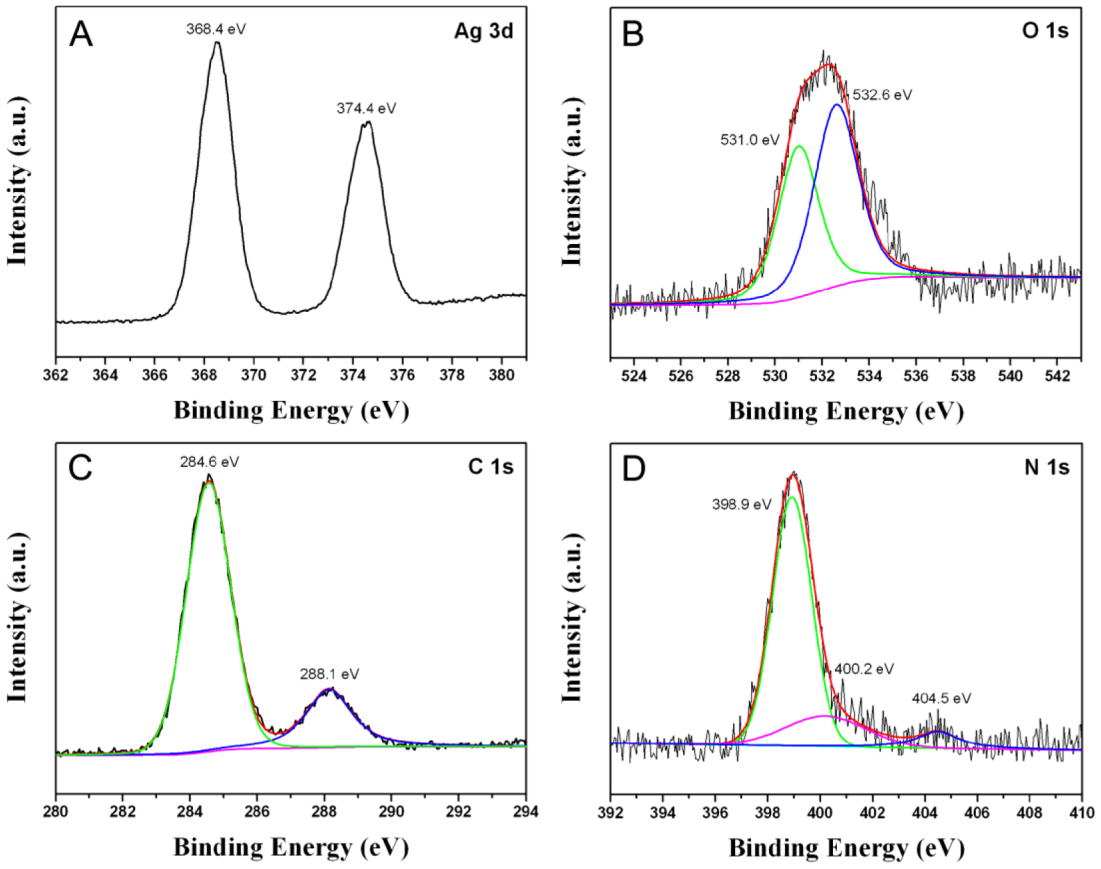

Figure 4. High resolution XPS spectra of the g-C_3N_4/Ag_2O (1:4) composite: (A) Ag 3d, (B) O 1s, (C) C 1s, and (D) N 1s.

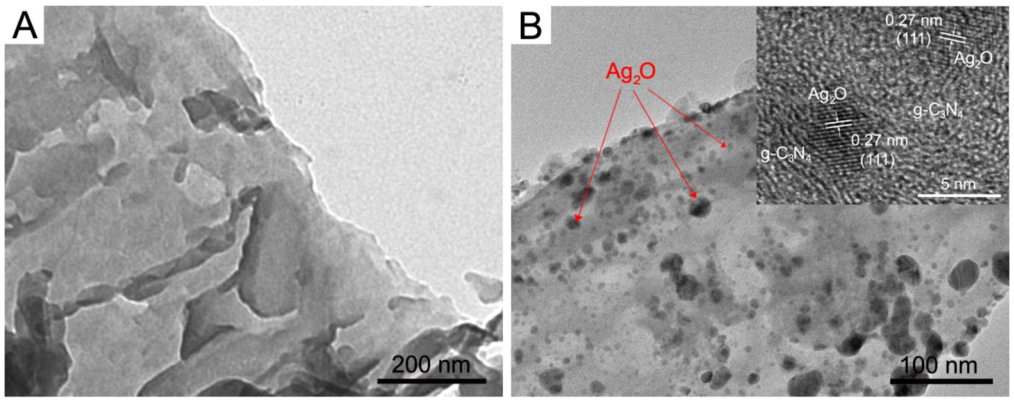

Figure 5. TEM images of (A) the pure g-C_3N_4 and (B) the g-C_3N_4/Ag_2O (1:4) composite (inset: HRTEM image of the composite).

separation efficiency and enhancing the photocatalytic activity. With decreasing ratio of g-C_3N_4 and Ag_2O, the particle size of Ag_2O increases slightly following with an obvious aggregation.

3.3. Optical Property of g-C_3N_4/Ag_2O Photocatalysts. The optical properties of the as-prepared g-C_3N_4, Ag_2O, and the g-C_3N_4/Ag_2O composites were measured via the UV−vis DRS technique. As shown in Figure 6, the absorption edge of the pure g-C_3N_4 is at about 460 nm, which originates from its band gap of ~2.69 eV and is consistent with the reported results.[28] After the introduction of Ag_2O nanoparticles on the surface of g-C_3N_4, the optical absorption of the composites in the visible region increases, while the absorption intensity of these composites is stepwisely strengthened with the increasing Ag_2O mass ratios. As for the as-prepared Ag_2O sample, it clearly exhibits a wide and strong light absorption in the whole UV−vis range of 200−800 nm, which is related to its excellent photocatalytic activity.[24,25] The results of UV−vis DRS suggest that the fabrication of the heterostructured g-C_3N_4/Ag_2O composites can greatly improve the optical absorption property and increase the utilized efficiency of solar light, which are favorable for the enhancement of the photocatalytic activity.

3.4. Photocatalytic Activity. The photocatalytic activities of the as-prepared g-C_3N_4/Ag_2O composites with different mass ratios were evaluated by the photodegradation of MO dye under visible light irradiation shown in Figure 7. For comparison, the activities of pure Ag_2O and g-C_3N_4 were also tested under the same conditions. The blank experiment indicates that the direct photolysis of MO is almost ignored in

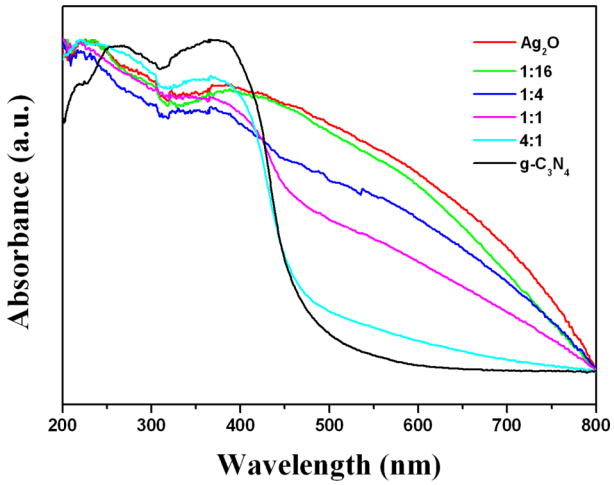

Figure 6. UV−vis DRS of the as-prepared g-C_3N_4, Ag_2O, and g-C_3N_4/Ag_2O composites.

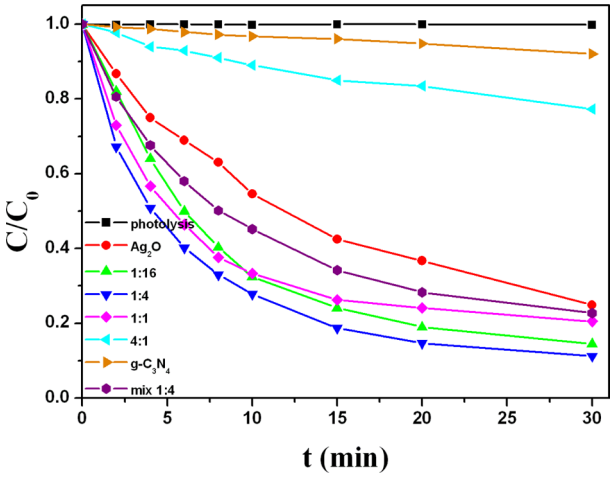

Figure 7. Visible light induced photocatalytic degradation efficiency of MO in the presence of as-prepared g-C_3N_4, Ag_2O, and g-C_3N_4/Ag_2O composites.

the absence of photocatalysts and the degradation of MO is resulted from the photocatalytic reaction. It can be clearly observed that when the mass ratio of g-C_3N_4 and Ag_2O is lower than 1:1, the as-prepared composites exhibit much higher photocatalytic activities than that of the pure g-C_3N_4 and Ag_2O. This may be caused by the formation of heterostructure between g-C_3N_4 and Ag_2O. Additionally, the improved dispersibility and the decreased particle size of Ag_2O shown in Figure S2 of the as-prepared composites also play important roles in enhancing photocatalytic activity. With respect to the g-C_3N_4/Ag_2O composites, the photocatalytic activities increase gradually with decreasing the mass ratios of g-C_3N_4 and Ag_2O from 4:1 to 1:4 and then decrease slightly at the mass ratio of 1:16. As the mass ratio of g-C_3N_4 and Ag_2O is 1:4, the composite shows the highest activity, which exceeds 1.2 times more than that of bare Ag_2O and 11 times larger than that of g-C_3N_4. In this photocatalytic reaction, nearly 50% of MO has been degraded in the first 4 min, and ∼90% of MO can be removed after 30 min. This result can be clearly observed in Figure 8. With extended time under visible light irradiation, the intensity of the peak at 463 nm, which is related to the characteristic UV−vis absorption of MO molecule, decreases

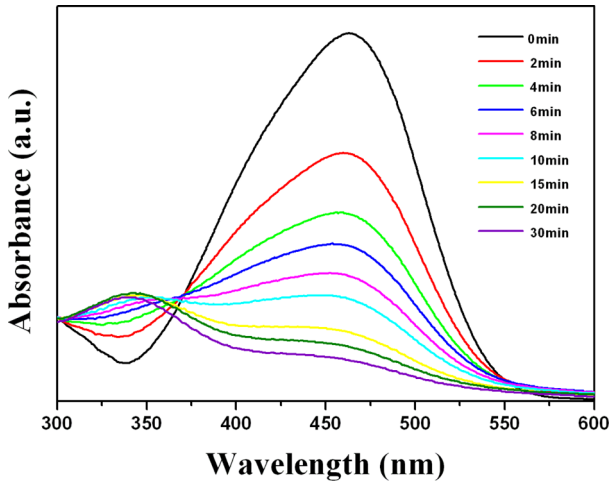

Figure 8. UV−visible absorption spectrum of MO dye after the corresponding degradation time over the g-C_3N_4/Ag_2O (1:4) composite.

stepwisely and almost disappears after 30 min. Further decreasing the mass ratio of g-C_3N_4 and Ag_2O to 1:16, the slightly decreased photocatalytic activity may be attributed to the fact that the higher content of Ag_2O may easily result in the agglomerate of Ag_2O particles causing a low dispersibility on the surface of g-C_3N_4. This may influence the transfer of photogenerated charge carriers as well as the separation efficiency of the photoinduced electron−hole pairs.[34] Consequently, a suitable ratio between g-C_3N_4 and Ag_2O is significant for effectively enhancing the photocatalytic activity. In order to substantiate the contribution of heterostructure on the photocatalytic activity, a reference experiment on the mechanically mixed g-C_3N_4 and Ag_2O with a mass ratio of 1:4 was also performed. The activity of the mechanically mixed sample shows higher than those of bare g-C_3N_4 and Ag_2O, but still much lower than those of as-prepared composites. The result strongly suggests that the intimate junctions between g-C_3N_4 and Ag_2O bring some synergistic reaction to enhance the photocatalytic activity of the g-C_3N_4/Ag_2O heterostructured photocatalysts. Therefore, the as-prepared g-C_3N_4/Ag_2O composite with the suitable mass ratio (1:4) can be regard as an effective photocatalyst, while its observed photocatalytic performance is much better than most of the reported nanoheterostructured photocatalysts for degradation MO under visible light irradiation.[25,27,38−41]

In addition, as shown in Figure S4, the phenol which has no absorbance in visible region was chosen as a probe molecule to further evaluate the visible-light activity of the as-prepared g-C_3N_4/Ag_2O (1:4) composite. After reacting of 180 min under the visible-light irradiation, no degradation in the direct photolysis of phenol and only 4% of phenol has been removed over the pure g-C_3N_4. In contrast, the g-C_3N_4/Ag_2O (1:4) composite reveals much improved activity that nearly 82% of phenol has been degraded after 180 min. The results further indicate that the as-prepared g-C_3N_4/Ag_2O (1:4) composite can be used as a high efficient visible-light photocatalyst.

Figure 9 displays the photoluminescence (PL) spectra of the as-prepared g-C_3N_4/Ag_2O composites together with that of bare g-C_3N_4 for comparison. All samples exhibit an emission peak centered at about 450 nm, which is similar to the reported value in the literatures.[31,42] Compared with g-C_3N_4, the g-C_3N_4/Ag_2O composites show significant quenching of the PL.

dx.doi.org/10.1021/am4038307 | ACS Appl. Mater. Interfaces 2013, 5, 12533−12540

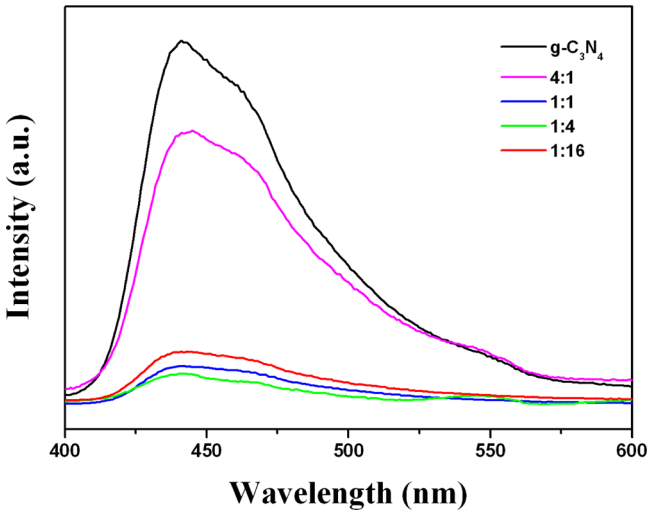

Figure 9. PL spectra of the as-prepared Ag_2O and g-C_3N_4/Ag_2O composites.

This result further indicates an efficient charge transfer within the g-C_3N_4/Ag_2O samples because the intensity of the PL peaks is related to the recombination of the electron−hole pairs within the semiconductor. In particular, when the mass ratio of g-C_3N_4 and Ag_2O is 1:4, the PL peak reveals the lowest intensity, which is well consistent with the result of the photocatalytic activity. That is to say, in the case of g-C_3N_4/Ag_2O (1:4) composite, the photogenerated electron−hole pairs can efficiently transfer at the interface of heterostructure, resulting in the highest photocatalytic activity under visible light irradiation.

3.5. Possible Photocatalytic Mechanism. Based on the results above, a possible photocatalytic mechanism of the as-prepared g-C_3N_4/Ag_2O composites under visible light irradiation was proposed and illustrated in Figure 10. As well known,

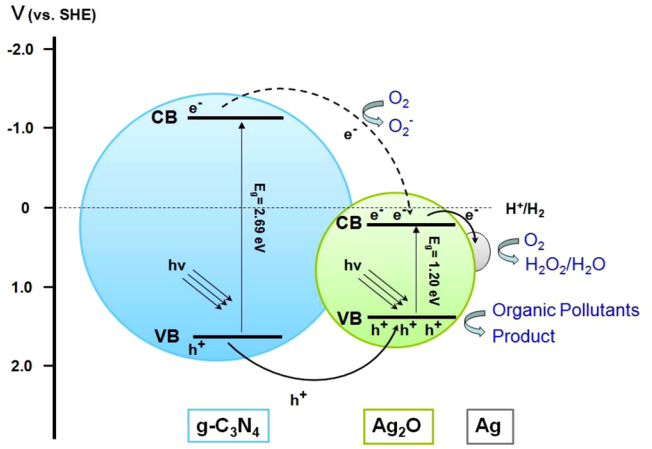

Figure 10. Schematic diagrams for the possible photocatalytic mechanism of the g-C_3N_4/Ag_2O composite under visible light irradiation.

Ag_2O is a typical *p*-type semiconductor, while g-C_3N_4 is *n*-type. Under visible light irradiation, both Ag_2O and g-C_3N_4 can be excited to generate electrons and holes. In the g-C_3N_4/Ag_2O composites, the photogenerated electrons will have a tendency to transfer from Ag_2O to g-C_3N_4 and the holes have an opposite transfer because of the inner electric field existed in the *p*−*n* junctions.[43] On the other hand, the conduction band (CB) bottom of g-C_3N_4 (−1.12 V, vs SHE) is more negative than that of Ag_2O (0.20 V, vs SHE) and the valence band (VB) top of g-C_3N_4 (1.57 V, vs SHE) is more positive than that of Ag_2O (1.40 V, vs SHE).[21,24] Considering the inner electric field and energy band structure, it is reasonable to conclude that the transfer of electrons between g-C_3N_4 and Ag_2O is partly restricted, while the transfer of holes can be accelerated. This causes an efficient separation of photogenerated electrons and holes to enhance the photocatalytic activity. The electrons on the CB of g-C_3N_4 may be captured by oxygen to generate active species due to its more negative CB position compared with the single electron reduction of oxygen ($O_2 + e^- + H^+ = HO_2$ (aq), −0.046 V vs SHE). In addition, due to the potentials of $^{\bullet}OH$/OH^- (1.99 V vs SHE), H_2O_2 (1.77 V vs SHE), and O_3 (2.07 V vs SHE) being more positive than the VB of Ag_2O, the enriched holes on the VB of Ag_2O can be consumed by directly decomposing the absorbed organic pollutants on the surface of the catalysts rather than generate the stronger oxidative species of $^{\bullet}OH$ radicals, H_2O_2, and O_3 during the photocatalysis, which is beneficial to decreasing the probability of the electron−hole recombination.[24,44,45] Furthermore, because of the more positive potential of Ag^+/Ag (0.7991 V, vs SHE), the photogenerated electrons on the CB of Ag_2O may in situ reduce Ag^+ to metallic Ag, which also acts as an electron pool and transfers the electron to oxygen via the multielectron-transfer routes ($O_2 + 2e^- + 2H^+ = H_2O_2$ (aq), 0.682 V vs SHE; $O_2 + 4e^- + 4H^+ = 2H_2O$ (aq), 1.23 V vs SHE).[24] In other words, the generated photoelectrons excited by the visible-light can transport to the surface of Ag_2O and the Ag^+ (Ag_2O) could be partly reduced to metallic Ag,[46] while the formed metallic Ag can further complete efficient electron migration process to efficiently inhibit the recombination of the photoexcited pairs. As a result, the photogenerated electron−hole pairs can be separated efficiently in the photocatalytic system of g-C_3N_4/Ag_2O heterostructure, leading to a significantly enhanced photocatalytic activity than the pure g-C_3N_4 and Ag_2O. Based on the above discussions, it can be concluded that the enhanced photocatalytic activity of the as-prepared g-C_3N_4/Ag_2O can be ascribed not only to the improved dispersibility and the deceased particle size of Ag_2O as well as the improved optical absorption property arising from the heterostructure between g-C_3N_4 and Ag_2O, but also to their synergetic effects of the inner electric field and matched energy band structure that bring the high separation rate of the photogenerated charge carriers.

3.6. Stability Evaluation. From the viewpoint of practical applications, the g-C_3N_4/Ag_2O composite with the mass ratio of 1:4 as the representative sample was selected to evaluate the reusability of the as-prepared composites. As shown in Figure 11, the as-prepared g-C_3N_4/Ag_2O composite shows a good catalytic stability, maintaining a similar level of reactivity after four cycles. The slight decrease should originate from the inescapable loss of catalyst during the recycling process.

The composition of the recyclable composite was also characterized by XRD. As shown in Figure S5, some new diffraction peaks appear, which can be ascribed to metallic Ag (JCPDS 04-0783). That indicates Ag^0 species can be formed during the photocatalytic process arising from the partial in situ photoreduction of Ag_2O due to the more positive potential of Ag^+/Ag (0.7991 V, vs SHE) compared with O_2/HO_2 (−0.046 V, vs SHE). Previous research results demonstrated that, after the formation of a certain amount of metallic Ag, the obtained

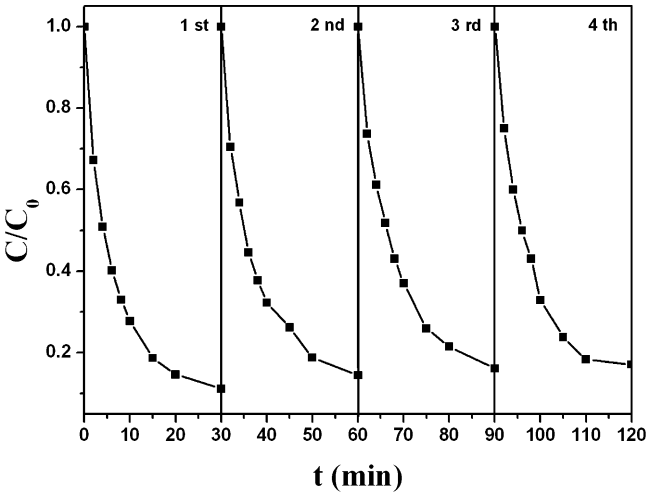

Figure 11. Circling runs in the presence of the g-C_3N_4/Ag_2O (1:4) composite for photodegradation of MO dye under visible light irradiation.

Ag_2O/Ag exhibits a stable structure.[24] Accordingly, the photogenerated electrons can easily transfer to the metallic Ag sites to restrict the recombination of photogenerated charge carriers resulting in enhanced photocatalytic activities. Therefore, the prepared g-C_3N_4/Ag_2O composites can be regard as a high activity and stability visible light photocatalyst, which show a great potential to be used in the field of environmental remediation.

4. CONCLUSIONS

In this paper, a series of g-C_3N_4/Ag_2O heterostructured photocatalysts with different mass ratios of g-C_3N_4 and Ag_2O were prepared by a simple liquid phase reaction method at room temperature. The photodegradation of MO experiments together with the PL analysis revealed that the mass ratio of g-C_3N_4 and Ag_2O showed a significant effect on the separation of photogenerated charge carriers as well as the visible light photocatalytic activity. The composite with the mass ratio of 1:4 degraded nearly 50% of MO within 4 min, and ~90% after 30 min. In addition, the prepared photocatalysts had relative stability under visible light irradiation. The enhanced photocatalytic activity of the g-C_3N_4/Ag_2O composites was mainly attributed to the synergetic effects between g-C_3N_4 and Ag_2O, as well as the improved dispersibility and the decreased particle size of Ag_2O. The results provided here not only offer a highly efficient and stable photocatalytic material for environmental remediation, but also shed a new insight for fabricating efficient heterostructured photocatalysts.

■ ASSOCIATED CONTENT

Supporting Information

High resolution XPS spectra of Ag 3d for the pure Ag_2O and N 1s for the pure g-C_3N_4. TEM images of the as-prepared g-C_3N_4/Ag_2O composites with different ratios. SEM images of the pure Ag_2O. Visible light induced photocatalytic degradation efficiency of the phenol. XRD patterns of the g-C_3N_4/Ag_2O (1:4) composite after the cycling photocatalytic experiments. This material is available free of charge via the Internet at http://pubs.acs.org.

■ AUTHOR INFORMATION

Corresponding Author

*E-mail: dongsj@ciac.ac.cn.

Notes

The authors declare no competing financial interest.

■ ACKNOWLEDGMENTS

This work was supported by the National Natural Science Foundation of China (No. 21375123 and 21075116) and the 973 Projects (2010CB933603, 2011CB911002).

■ REFERENCES

(1) Chen, X.; Mao, S. S. *Chem. Rev.* **2007**, *107*, 2891−2959.
(2) Zhang, H.; Lv, X. J.; Li, Y. M.; Wang, Y.; Li, J. H. *ACS Nano* **2010**, *4*, 380−386.
(3) Lin, H.; Li, L.; Zhao, M.; Huang, X.; Chen, X.; Li, G.; Yu, R. *J. Am. Chem. Soc.* **2012**, *134*, 8328−8331.
(4) Zuo, F.; Bozhilov, K.; Dillon, R. J.; Wang, L.; Smith, P.; Zhao, X.; Bardeen, C.; Feng, P. *Angew. Chem., Int. Ed.* **2012**, *51*, 6223−6226.
(5) Li, H.; Wang, D.; Wang, P.; Fan, H.; Xie, T. *Chem.—Eur. J.* **2009**, *15*, 12521−12527.
(6) Wu, G.; Wen, J.; Nigro, S.; Chen, A. *Nanotechnology* **2010**, *21*, 85701−85706.
(7) Zhou, J. K.; Lv, L.; Yu, J. Q.; Li, H. L.; Guo, P. Z.; Sun, H.; Zhao, X. S. *J. Phys. Chem. C* **2008**, *112*, 5316−5321.
(8) Zhang, Y.; Tang, Y.; Liu, X.; Dong, Z.; Hng, H. H.; Chen, Z.; Sum, T. C.; Chen, X. *Small* **2013**, *9*, 996−1002.
(9) Wang, H.; Gao, J.; Guo, T.; Wang, R.; Guo, L.; Liu, Y.; Li, J. *Chem. Commun.* **2012**, *48*, 275−277.
(10) Wang, H.; Bai, Y.; Yang, J.; Lang, X.; Li, J.; Guo, L. *Chem.—Eur. J.* **2012**, *18*, 5524−5529.
(11) Wang, X.; Maeda, K.; Thomas, A.; Takanabe, K.; Xin, G.; Carlsson, J. M.; Domen, K.; Antonietti, M. *Nat. Mater.* **2009**, *8*, 76−80.
(12) Dong, F.; Wu, L. W.; Sun, Y. J.; Fu, M.; Wu, Z. B.; Lee, S. C. *J. Mater. Chem.* **2011**, *21*, 15171−15174.
(13) Dong, F.; Sun, Y. J.; Wu, L. W.; Fu, M.; Wu, Z. B. *Catal. Sci. Technol.* **2012**, *2*, 1332−1335.
(14) Zheng, Y.; Liu, J.; Liang, J.; Jaroniec, M.; Qiao, S. Z. *Energy Environ. Sci.* **2012**, *5*, 6717−6731.
(15) Li, X. H.; Wang, X. C.; Antonietti, M. *Chem. Sci.* **2012**, *3*, 2170−2174.
(16) Niu, P.; Zhang, L. L.; Liu, G.; Cheng, H. M. *Adv. Funct. Mater.* **2012**, *22*, 4763−4770.
(17) Han, K. K.; Wang, C. C.; Li, Y. Y.; Wan, M. M.; Wang, Y.; Zhu, J. H. *RSC Adv.* **2013**, *3*, 9465−9469.
(18) Wang, X. C.; Chen, X. F.; Thomas, A.; Fu, X. Z.; Antonietti, M. *Adv. Mater.* **2009**, *21*, 1609−1612.
(19) Sun, L.; Zhao, X.; Jia, C. J.; Zhou, Y.; Cheng, X.; Li, P.; Liu, L.; Fan, W. *J. Mater. Chem.* **2012**, *22*, 23428.
(20) Liu, W.; Wang, M. L.; Xu, C. X.; Chen, S. F.; Fu, X. L. *J. Mol. Catal. A: Chem.* **2013**, *368*, 9−15.
(21) Yan, S. C.; Lv, S. B.; Li, Z. S.; Zou, Z. G. *Dalton Trans.* **2010**, *39*, 1488−1491.
(22) Ye, S.; Qiu, L. G.; Yuan, Y. P.; Zhu, Y. J.; Xia, J.; Zhu, J. F. *J. Mater. Chem. A* **2013**, *1*, 3008−3015.
(23) Li, Y.; Zhang, H.; Liu, P.; Wang, D.; Li, Y.; Zhao, H. *Small* **2013**, *9*, 3336−3344.
(24) Wang, X.; Li, S.; Yu, H.; Yu, J.; Liu, S. *Chem.—Eur. J.* **2011**, *17*, 7777−7780.
(25) Zhou, W.; Liu, H.; Wang, J.; Liu, D.; Du, G.; Cui, J. *ACS Appl. Mater. Interfaces* **2010**, *2*, 2385−2392.
(26) Wu, M.; Yan, J. M.; Zhao, M.; Jiang, Q. *ChemPlusChem* **2012**, *77*, 931−935.
(27) Yu, H. G.; Liu, R.; Wang, X. F.; Wang, P.; Yu, J. G. *Appl. Catal., B* **2012**, *111*, 326−333.
(28) Yan, S. C.; Li, Z. S.; Zou, Z. G. *Langmuir* **2009**, *25*, 10397−10401.

(29) Fu, J.; Tian, Y. L.; Chang, B. B.; Xi, F. N.; Dong, X. P. *J. Mater. Chem.* **2012**, *22*, 21159−21166.
(30) Bojdys, M. J.; Muller, J. O.; Antonietti, M.; Thomas, A. *Chem.—Eur. J.* **2008**, *14*, 8177−8182.
(31) Kumar, S.; Surendar, T.; Baruah, A.; Shanker, V. *J. Mater. Chem. A* **2013**, *1*, 5333−5340.
(32) Bosca, M.; Pop, L.; Borodi, G.; Pascuta, P.; Culea, E. *J. Alloys Compd.* **2009**, *479*, 579−582.
(33) Lucacel, R. C.; Marcus, C.; Timar, V.; Ardelean, I. *Solid State Sci.* **2007**, *9*, 850−854.
(34) Huang, L.; Xu, H.; Li, Y.; Li, H.; Cheng, X.; Xia, J.; Xu, Y.; Cai, G. *Dalton Trans.* **2013**, *42*, 8606−8616.
(35) Yan, H.; Chen, Y.; Xu, S. *Int. J. Hydrogen Energy* **2012**, *37*, 125−133.
(36) Yan, S. C.; Li, Z. S.; Zou, Z. G. *Langmuir* **2010**, *26*, 3894−3901.
(37) Xu, H.; Yan, J.; Xu, Y.; Song, Y.; Li, H.; Xia, J.; Huang, C.; Wan, H. *Appl. Catal., B* **2013**, *129*, 182−193.
(38) Cao, J.; Xu, B.; Luo, B.; Lin, H.; Chen, S. *Catal. Commun.* **2011**, *13*, 63−68.
(39) Cheng, H.; Huang, B.; Dai, Y.; Qin, X.; Zhang, X. *Langmuir* **2010**, *26*, 6618−6624.
(40) Cao, S. W.; Yin, Z.; Barber, J.; Boey, F. Y.; Loo, S. C.; Xue, C. *ACS Appl. Mater. Interfaces* **2012**, *4*, 418−423.
(41) Cao, J.; Li, X.; Lin, H.; Xu, B.; Chen, S.; Guan, Q. *Appl. Surf. Sci.* **2013**, *266*, 294−299.
(42) Liao, G.; Chen, S.; Quan, X.; Yu, H.; Zhao, H. *J. Mater. Chem.* **2012**, *22*, 2721−2726.
(43) Li, L.; Xu, L.; Shi, W.; Guan, J. *Int. J. Hydrogen Energy* **2013**, *38*, 816−822.
(44) Jiang, Z.; Yang, F.; Yang, G.; Kong, L.; Jones, M. O.; Xiao, T.; Edwards, P. P. *J. Photochem. Photobiol., A* **2010**, *212*, 8−13.
(45) Ge, L.; Han, C.; Liu, J.; Li, Y. *Appl. Catal., A* **2011**, *409−410*, 215−222.
(46) Zhang, H.; Wang, G.; Chen, D.; Lv, X.; Li, J. *Chem. Mater.* **2008**, *20*, 6543−6549.